BOLETIN DE LA SOCIEDAD ESPAÑOLA DE
Cerámica y Vidrio
www.elsevier.es/bsecv

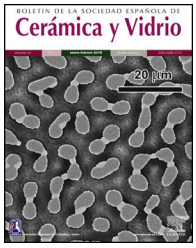

Judd–Ofelt and luminescence study of Dysprosium-doped lithium borosilicate glasses for lasers and w-LEDs

Ismail Kashif[a,*], *Asmaa Ratep*[b]

[a] *Physics Department, Faculty of Science, Al-Azhar University, Nasr City, Cairo, Egypt*
[b] *Department of Physics, Faculty of Women for Art, Science & Education, Ain Shams University, Heliopolis, Cairo, Egypt*

ARTICLE INFO

Article history:
Received 27 January 2021
Accepted 2 June 2021
Available online 19 June 2021

Keywords:
X-ray diffraction
FTIR
Optical spectroscopy
Judd–Ofelt parameters
CIE chromaticity

ABSTRACT

The effect of Dysprosium concentration has been studied in glasses of the system 30 SiO_2 + 30 Li_2O + (40−x) B_2O_3 + x Dy_2O_3 glass system where x = 0.5, 1, 2.5, 5 and 10 mol%. FT-IR studies were performed to understand the functional groups of the network involved in the host glass. The optical band gap is found in the range of 3.84–3.5 eV. From the absorption spectra, the experimental data were compared with the theoretical data computed by Judd–Ofelt theory. Nephelauxetic ratio (β) and bonding parameters (δ) computed using the absorption spectrum. The Judd–Ofelt parameters ($\Omega 2$, $\Omega 4$, and $\Omega 6$) obtained demonstrates the covalent and asymmetric nature of dysprosium ions. From the visible emission spectra, the intensity ratios were calculated from yellow to blue and the relative differences were discussed based on the concentration of Dy^{3+} ions. CIE chromaticity coordinates were calculated for all glass samples. A CIE chromatogram shows a glass containing 0.5 mol% Dy_2O_3 with color coordinates X = 0.32 and Y = 0.33 with the highest emission intensity. These glasses have great potentials for lasers and white LEDs (Light-Emitting Diode) applications.

Judd-Ofelt y estudio de luminiscencia de vidrios de borosilicato de litio dopados con disprosio para láseres y w-LED

Palabras clave:
Difracción de rayos X
FTIR
Espectroscopia óptica
Parámetros Judd-Ofelt
Cromaticidad CIE

RESUMEN

Se ha estudiado el efecto de la concentración de disprosio en vidrios del sistema 30 SiO_2 + 30 Li_2O + (40-x) B_2O_3 + x Dy_2O_3, donde x = 0,5%, 1%, 2,5%, 5% y 10% en moles. Los estudios de FT-IR se realizaron para investigar y entender los grupos funcionales de la red que compone el vidrio. La banda prohibida óptica se encuentra entre 3,84 y 3,5 eV.

* *Corresponding author.*
E-mail address: ismailkashif52@yahoo.com (I. Kashif).
https://doi.org/10.1016/j.bsecv.2021.06.001

Observando los espectros de absorción, los datos experimentales se compararon con los cálculos teóricos computados con la teoría de Judd-Ofelt. El nephelauxetic ratio (β) y los parámetros de unión (δ) se calcularon utilizando los espectros de absorción. Los parámetros (Ω2, Ω4 y Ω6), obtenidos mediante Judd-Ofelt, demuestran el carácter covalente y asimétrico de los iones de disprosio. A partir de los espectros de emisión visible se calcularon las relaciones de intensidad desde amarillo hasta azul, y se discutieron las diferencias relativas, basándose en la concentración de iones Dy^{3+}. Se calcularon las coordenadas de cromaticidad CIE para todas las muestras de vidrio. El cromatograma CIE correspondiente a un vidrio que contiene 0,5% en moles de Dy_2O_3 muestra coordenadas de color X = 0,32 y Y = 0,33, con la mayor intensidad de emisión. Este conjunto de vidrios tiene un gran potencial para su posible uso en aplicaciones como láseres y LED blancos.

Introduction

With the industrial progress that mankind is moving into, the frequent use of lighting and luminous devices such as phones and laptops, and the reduced exposure of humans to solar radiation, have negatively affected human health [1]. Moreover the usages of lightning in the optical fiber communication [2]. This attracted attention to the manufacture of a luminous material that had color-balance properties [3].

The shielding around 4f shell of RE (rare-earth) by the outer 5S and 5P shell caused the sharp fluorescence in the ultraviolet (UV), to infrared (IR) regions [4]. From all the RE elements Dysprosium Dy was chosen as it excited under UV wavelength and emitted two intense emission peaks [5], in the blue B region ($^4F_{9/2} \rightarrow {}^6H_{15/2}$) at 484 nm and yellow Y region ($^4F_{9/2} \rightarrow {}^6H_{13/2}$) at 574 nm. The combination between two peaks formed white light investigated by the Y/B ratio. The Y/B ratio can be changed and adjusted by changing the chemical composition, pumping of wavelengths, and Dy^{3+} ion content [5].

Better emission properties with long durability it is achieved using the host selection. Borosilicate glasses provide a wide range of composition, lower thermal expansion, high chemical stability, and good rare earth solubility [4,6].

The incorporation of alkali or alkaline earth metals to borosilicate glass system form non-bridging oxygen (NBOs) that decreases the connectivity of melts [6].

Moreover many studies carried on the production of white color as, D.D. Ramtek et al. studied the physical and optical properties of lithium borosilicate glasses doped with Dy3+ ions and found the two concentrations 1.5 mol% and 2 mol% Dy have the value (0.34, 0.35) chromaticity could be reached to a pure white light [7]. Dy^{3+} doped lithium aluminum borate glasses for W-LEDs studied by P.P. Bauer et al. [4]. It was found that the glass sample containing 0.5 mol% Dy_2O_3 had the highest emission intensity with color coordinates $X = 0.34$ and $Y = 0.38$.

D.D. Ramteke et al. [8] studied the Sm^{3+}/Dy^{3+} doped lithium borosilicate glasses and found that the emission intensity increased with increasing Dy^{3+} content.

The aim of this work to study the effect of substitution a former like boron with rare earth Dy in the presence of a constant alkali silicate concentration on optical white emission.

Experimental

Glass compositions 30 SiO_2 + 30 Li_2O + (40−x) B_2O_3 + x Dy_2O_3 where x = 0.5, 1, 2.5, 5 and 10 mol% were fabricated via the melt quenching technique. The samples were melted in a porcelain crucible at 300 °C for half an hour and 1050 °C in an electric muffle furnace (LENTON) and poured it immediately between two copper plates.

The samples were examined by using Philips Analytical X-ray diffraction system, type PW3710 based on Cu tube anode of wavelength $K_{\alpha 1} = 1.5406$ Å and $K_{\alpha 2} = 1.54439$ Å. The starting angle was 10° and the end angle 70°. The step size was 0.05° and the time per step was 2.5 s. XRD showed no evidence of crystals in all glass samples.

The room temperature glass density (ρ) was determined using an Archimedes method with toluene (99.99% purity) as the immersion liquid. The density yield:

$$\rho = \frac{(0.865Wa)}{(Wa - Wb)}\ \mathrm{g\ cm^{-3}} \quad (1)$$

where Wa and Wb are the weight of glass samples in air and toluene respectively, and 0.865 g cm^{-3} is the density of toluene at room temperature.

The FTIR absorption spectra of the prepared samples were measured at room temperature in the range 2000–400 cm^{-1} by an infrared spectrometer (type JASCO FTIR-4100, Japan) using the KBr disk technique.

The comparative changes in both BO3 and BO4 units can be verified from the calculation of the appreciable fraction of $[BO_4]$ and $[BO_3]$ units can be calculated by the following equation:

$[BO_4]$ = Sum of the specific areas of corresponding BO_4 units at (920 − 980 − 1080 cm^{-1})

$[BO_3]$ = Sum of the specific areas of corresponding BO_3 units at (1200 − 1600 cm^{-1}).

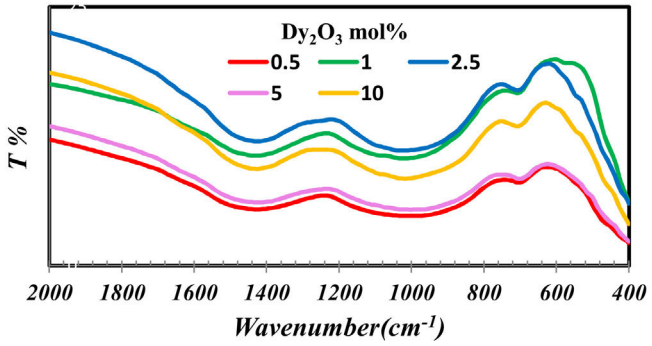

Fig. 1 – The FTIR of borosilicate glass samples with different concentrations of Dy_2O_3.

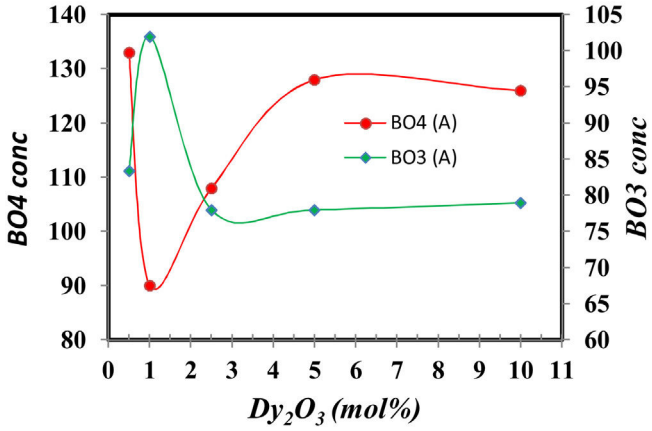

Fig. 2 – The BO_3 and BO_4 relation of glass samples.

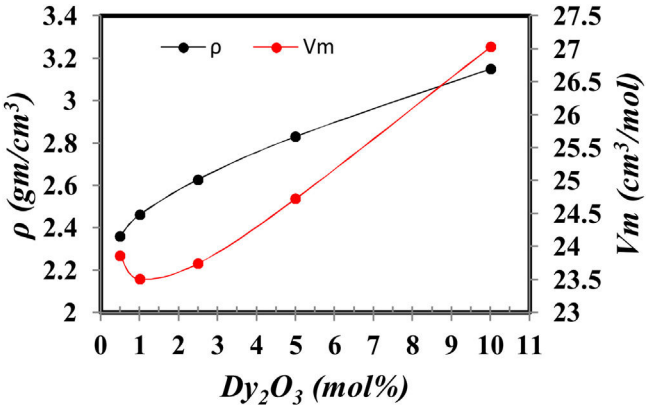

Fig. 3 – The Density and molar volume of glass samples.

The optical absorption spectra were measured in the range from 190 to 2500 nm using a computerized recording spectrophotometer (type JASCO, V-570).

The emission measurements were carried out using (JASCO-FP-6300) Spectrofluorometer in the wavelength range (200–800 nm).

Results and discussion

The importance of FTIR is concentrated in studying the groups formed in the glass network. Fig. 1 indicates the FTIR of borosilicate glass samples with different concentrations of Dy_2O_3. From fig. 1 observed that the presence of broadband indicates the homogeneity of the glass and overlapped the borate groups with silicate. The borate groups identified with three region 1200–1600 cm^{-1} [9–11], the region 800–1200 cm^{-1} [9,10] and at 600–800 cm^{-1} [12]. The possible silicate groups in the glass network are Q4 (4 bridging oxygen) (1200 cm^{-1}), Q3 (3 bridging oxygen and one non-bridging) (1075 cm^{-1}), Q2 (2 bridging oxygen and 2 non-bridging) (1000 cm^{-1}), and Q1 (1 bridging oxygen and 3 non-bridging) (900 cm^{-1}). Besides these silicate groups, the broadband also contains a range of stretching vibrations for the Si—O—Si bonds [13,14] and the bending vibrations of bridging oxygen between boron atoms (B—O—B bonds) in BO_3 triangles [17]. The presence of silicate in the glass structure can be overlapped with borate groups in their region and formed the band from 830 to 1109 cm^{-1}. Intended for asymmetric stretching vibrations of Si—O—Si of [SiO_4] [10,11,15]. The band at 688 cm^{-1} attributed to the symmetric Si—O—Si stretching vibrations of the silicon tetrahedral group [12].

The silicate and borate groups could be connected as B—O—Si in the range 1105–1118 cm^{-1} and in 718 cm^{-1} [16,17]. The bands in the low wavenumber nearly at 460–550 nm represent the metallic cations vibration such as Dy^{3+} and Si^{4+} peak [9,11,12,15].

The FTIR spectra are also used to determine the $BO_3$and BO_4 concentrations from the deconvolution method.

FTIR spectra are used in determining the borate area, as seen in Fig. 1. From Fig. 2 it observes that the BO_3 and BO_4 have an opposite trend. It observes the destruction of the BO_3 vibration group into an asymmetric BO_4 vibration group associated with non-bridging oxygen. This glass consists of two former components, namely, SiO_2 and B_2O_3 with structural units [BO_3], [BO_4], and [SiO_4] attached to each other to form stable structural groups [12].

Density is an important tool to explain the structural modification in glass formation. Besides, the molar volume V_m plains the oxygen dispersion in the glass lattice [18].

Fig. 3 shows the variation of density and V_m ($V_m = M/\rho$ M is the molecular of sample composition) with the increase of Dy_2O_3 at the expense of B_2O_3. The density increases as the substituting the lower molecular weight B_2O_3 with the higher molecular weight Dy_2O_3 and formation of BO_4 that has a higher density than BO_3 [7,10]. The molar volume decreases up to 1 mol% Dy_2O_3 and then increases. The molar volume increases with Dy_2O_3 concentration due to it enters the glass network as the modifier occupies the interstitial position. As a result, the glass network expands. Or another explanation, the addition of Dy_2O_3 to glass samples change in the ratio of boron to oxygen and silicon to oxygen, which increases the cross-links of a group of borates and silicates, which leads to the expansion of the glass network, which causes an increase in the molar volume [7].

The compactness comparison of the prepared samples could be explained from the calculation, excess volume (V_e)

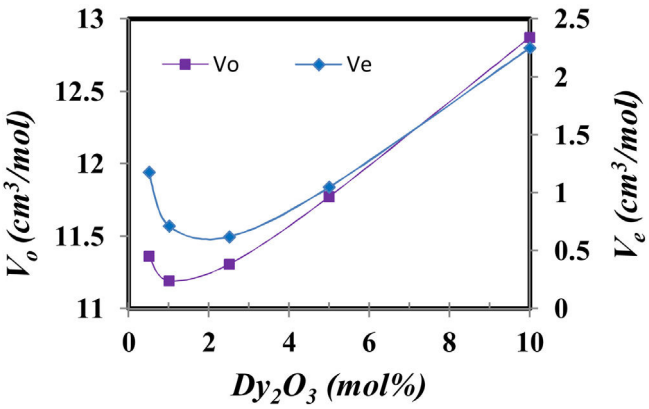

Fig. 4 – The Excess volume (V_e) and oxygen molar volume (V_o) of glass samples.

and oxygen molar volume (V_o) by the following equations [12] and the obtained results drawn in Fig. 4.

$$V_e = V_m - \sum_i x_i V_{m(i)} \tag{2}$$

$$V_o = \left(\sum \frac{x_i M_i}{\rho_{sample}}\right)\left(\frac{1}{\sum x_i n_i}\right) \tag{3}$$

where $V_{m(i)}$ is the molar volume of each oxide (M_{Wt}/ρ of each oxide), x_i is molar concentration of each oxide, M_i is molecular weight of each oxide (M_{Wt}), and n_i. is number of oxygen in each oxide.

Fig. 5 illustrates the scanning electron microscope (SEM) images of Dy^{3+} doped lithium borosilicate glass samples (1 and 10 mol% Dy_2O_3) and the percentages of the elements present in the studied glass samples obtained using the Energy Dispersive X-ray spectra (EDS). The morphologies of these glass samples do not show any grains, confirming the amorphous nature of the glass sample. The formation of crack results from the strain. This information agrees with the XRD results. It is indicated that the prepared glass samples are purely amorphous in nature.

The UV–Vis–NIR absorption spectra of all glass samples are shown in Fig. 6. Fig. 6 clears the intensity change of bands in the range in visible and NIR that characterize the Dy_2O_3 concentration, assigned for the transitions between the levels in $^4f_{9/2}$ electronic configuration from $^6H_{15/2}$ ground state to excited levels of Dy^{3+} ions [13,19].

The electronic structure from the optical absorption is used in determining many parameters as optical band gap, Nephelauxetic ratio (β), bonding parameter (δ), and the oscillator strength that is used to know the radiative properties.

A differentiation method is used to determine the optical band gap E_g by relationship [20].

$$\frac{d[\ln(\alpha h\nu)]}{d(h\nu)} = \frac{r}{h\nu - E_g} \tag{4}$$

where $\alpha(\upsilon)$ is the absorption coefficient, $h\nu$ is photon energy, and r is the type of transition.

The calculated E_g drew in Fig. 7.

From Fig. 7 it is observed that the optical band gap increase with the Dy_2O_3 concentration up to 2.5 mol% and then decreases. The change in the E_g values with concentration could be explained from the view of the structure change. From the results obtained, it was observed that the change of BO_4 and the molar size of both have an opposite behavior to the gap of the light beam with increasing the proportion of samples. It increases bonding and does not bridge the oxygen imbalance. This leads to an increase in the degree of localization of the electrons and thus an increase in the donor center in the vitreous matrix [12,21–24].

The nature of bonding between ligand around Dy determined from the nephaulextic ratio B, which evaluated from the ratio between the transition energy in the glass sample to the energy in the aqueous solution according to the relation $B = \upsilon c/\upsilon a$. The type of bonding (covalent or ionic) could be determined from the sign given from bonding parameter relation $\delta = (1 - B')/B'$ where $B' = \sum B/\text{number of transition } (n)$. The calculated values tabulated in Table 1, the negative sign that represents the iconicity nature of Dy^{3+} ligand bond in any hosts [19,25].

The spectral strength (f_{exp}) of absorption bands of glass composition doped with rare earth (Dy_2O_3) calculated from the integrated area under the peaks according to the relation

$$f_{\exp} = 4.32 \times 10^{-9} \int \alpha(\upsilon)\, d\upsilon \tag{5}$$

With the Judd–Ofelt theory, the spectral strength calculated theatrically according to the relation

$$f_{cal} = \frac{8\pi^2 mc\upsilon}{3hc^2(2J+1)}\left[\frac{(n^2+2)^2}{9n}\right]\sum_{\lambda=2,4,6}\Omega_\lambda |\langle aJ\|U^\lambda\|bJ'|\rangle|^2 \tag{6}$$

where Ω_λ is the Judd–Ofelt intensity parameters and h is Plank constant, n is the refractive index, m is the mass of electron, c is the speed of light and υ is frequency of transition. $\|U^\lambda\|$ are the reduced matrix elements due to J–J' transition of Dy^{3+}.

The quality fit between the results obtained experimentally and theoretically obtained from the root mean square equation according to the relation

$$\delta_{rms} = \left[\frac{\sum (f_{\exp} - f_{cal})^2}{N-3}\right]^{1/2} \tag{7}$$

where N is the number energy level.

The lower root mean square values δ_{rms} represent the agreement of the experimental values f_{exp} with the calculated values f_{cal} (Table 2).

The importance of Judd–Ofelt parameters derived from the absorption spectra, refractive index summarized in predict the glass structure and the fluorescence intensity of the transition [19,26].

The Judd–Ofelt parameters [27] indicate the glass structure, the Ω_2 indicate the short-range parameter as the covalence and asymmetry around Dy, while Ω_4 and Ω_6 show the long rang parameters as the rigidity and viscosity of glass samples.

Fig. 8 shows the relation between the Judd Ofelt parameters and the intensity of Dy_2O_3 concentration.

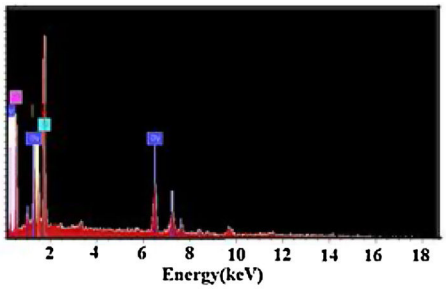

Energy keV

Element	Mass %	Atom%
Oxygen	35.98	42.56
Silicon	37.34	24.49
Boron	18.26	31.97
Dysprosium	8.42	0.98
Sum	100	100

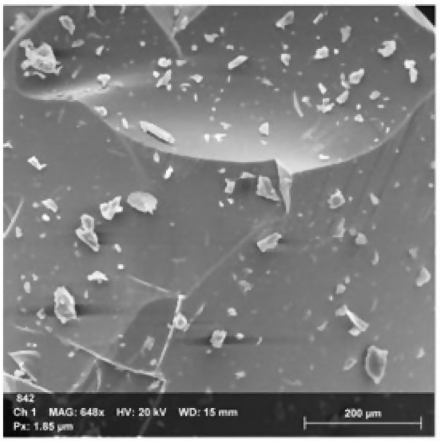

1 Dy_2O_3

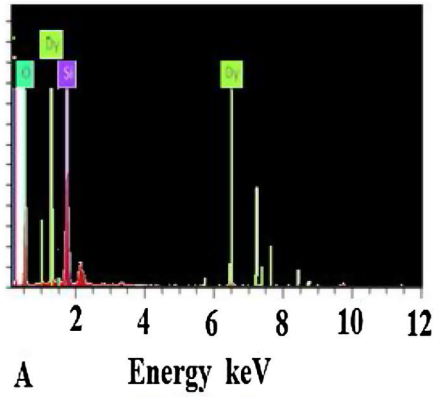

A Energy keV

Element	Mass %	Atom%
Oxygen	20.98	41.36
Silicon	23.00	25.1
Boron	8.31	24.2
Dysprosium	47.71	9.22
Sum	100	100

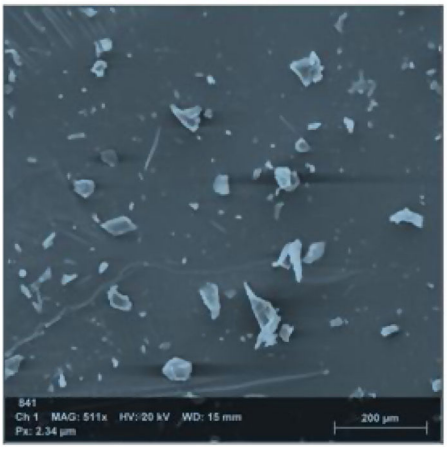

10 Dy_2O_3

Fig. 5 – Illustrates the scanning electron microscope (SEM) images of Dy^{3+} doped lithium borosilicate glass samples (1 and 10 mol% Dy_2O_3) and the percentages of the elements present.

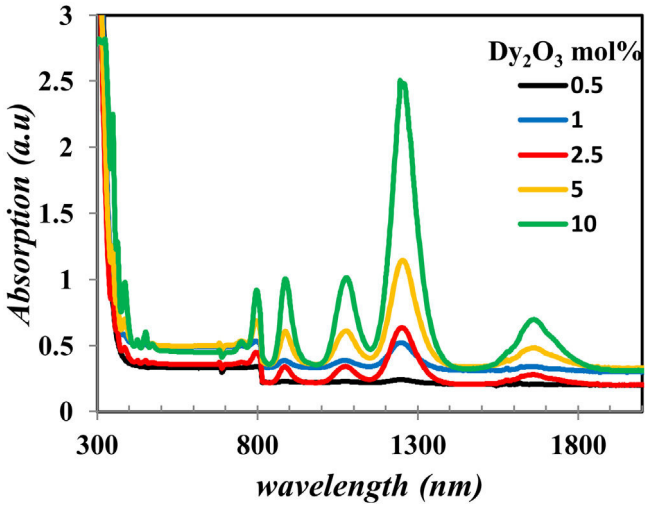

Fig. 6 – The optical absorption spectra of glass samples.

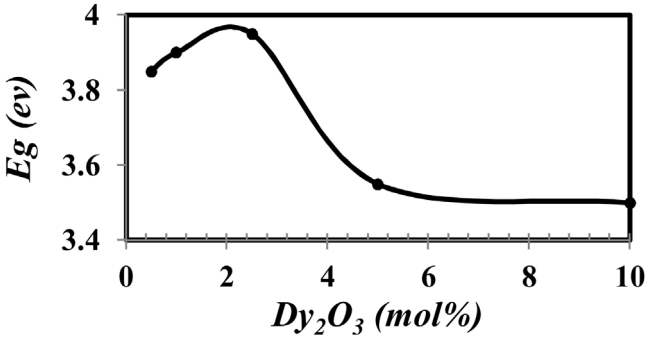

Fig. 7 – The optical band gap of the prepared glass samples.

Fig. 8 generally shows higher values of Ω_2 which represent a higher covalent around Dy, high disorder around Dy^{3+} and the host [28]. And it gradually decreases as the concentration of Dy ions increases. Fig. 8 demonstrates the opposite behavior between the decrease in covalency represented from Ω_2 value and the increase of ionicity represented from δ value that coincidence with the increase in BO^{4-} shown in fig. 2. Also, find that the parameter Ω_2, as well as the nephelauxetic (Table 1), has asymmetric behavior confirming that the increase in the coordination of BO4 reduces the asymmetry around Dy ions in the prepared glass [25].

The stimulated emission [29,30] of glass sample doped with Dy^{3+} characterized by the quality factor (Ω_4/Ω_6), which is important in explaining the behavior of laser transitions [17] tabulated in Table 3 matrix. It was found that the values of Ω_4/Ω_6 in Table 3 increased with increasing Dy^{3+} concentration to reach a value larger than 1 in the 10 mol% Dy_2O_3 as it predicts the possibility of laser emission. Judd–Ofelt parame-

Table 1 – The band positions (nm) of (the prepared glass samples and the aqua ion) and bonding parameters (β and δ) of the Dy^{3+} doped lithium borosilicate glasses.

λ_{nm}	10 Dy_2O_3	5 Dy_2O_3	2.5 Dy_2O_3	1 Dy_2O_3	0.5 Dy_2O_3	Aqua ion
1254	7974.48	7936.5	7936.5	7961.7	7898.8	7700
1084	9225.09	9208.1	9174.3	9225.09	9107.4	9100
892	11,210.76	11,235.95	11185.6	11235.9	11086.4	11000
800	12500	12500	12468.8	12531.3	12500	12400
770	12987	12987	13157.89	–	–	13250
476	21008.4	21008.4	–	21097	–	21100
454	–	–	–	–	22026.4	22100
428	23364.48	23474.17	23364.48	23474.17	23474.1	23400
388	25773.2	25906.73	25906.73	26,041.66	–	25,800
362	27,624.3	27,624.3	27,624.31	–		27,503
348	–	–	28,901.73	–	–	28,551
B'	1.006	1.0066	1.008	1.013	1.007	
δ	−0.006	−0.0065	−0.008	−0.013	−0.007	

Table 2 – The experimental spectral strength (f_{exp}) and calculated (f_{cal}) of absorption bands of glass composition and the values of root mean square (δ_{rms}) of absorption bands of the glass composition.

	10 Dy_2O_3		5 Dy_2O_3		2.5 Dy_2O_3		1 Dy_2O_3	
λ nm	f_{exp}	f_{cal}	f_{exp}	f_{cal}	f_{exp}	f_{cal}	f_{exp}	f_{cal}
1258	58.5	58.4	51.8	51.6	58.2	58.1	62.6	61.8
1086	12.6	12.6	11	10.8	11.6	11.3	12.2	11.2
892	8.89	8.82	7.79	8.40	8.19	9.43	8.60	12.3
800	3.84	3.74	5.07	3.79	6.94	4.44	13.6	6.51
770	0.2177	0.686	0.288	0.713	0.149	0.835	–	–
476	0.08	0.655	0.072	0.63	0.104	0.712	0.102	0.945
428	0.134	0.303	0.130	0.304	0.149	0.353	0.204	0.115
388	1.31	1.27	1.09	1.20	0.953	1.39	0.612	1.77
362	0.404	1.67	1.09	1.69	0.342	1.98	0.102	2.90
δ_{rms}	0.89		0.324		1.29		0.39	

Table 3 – The spectroscopic quality factor (Ω_4/Ω_6), Y/B ratio, (x, y) chromaticity and CCT at the excitation λ_{exc} = 350, 370, 390 nm.

Glass	Ω_λ (λ = 2, 4 and 6) $\Omega^* 10^{-20}$ cm^2	Trend	Reference	Ω_4/Ω_6
Lithium borosilicate 1.0Dy	52.8, 0.775, 10.6	$\Omega2 > \Omega6 > \Omega4$	P.W.	0.073
Lithium borosilicate 2.5Dy	46.6, 5.33, 7.26	$\Omega2 > \Omega6 > \Omega4$	P.W.	0.734
Lithium borosilicate 5.0Dy	37.0, 5.62, 5.69	$\Omega2 > \Omega6 > \Omega4$	P.W.	0.988
Lithium borosilicate 10.0Dy	40.7, 7.9, 5.55	$\Omega2 > \Omega4 > \Omega6$	P.W.	1.423
Tellurite	1.46, 2.32, 3.60	$\Omega6 > \Omega2 > \Omega4$	[31]	0.64
(Tellurite)	16.0, 2.39, 3.75	$\Omega2 > \Omega4 > \Omega6$	[3]	0.64
(Borate)	23.02,12.86,12.17	$\Omega2 > \Omega4 > \Omega6$	[32]	1.06
(Germanate)	3.65, 0.65, 1.57	$\Omega2 > \Omega6 > \Omega4$	[30]	0.41
Aluminoborosilicate Dy 0.1	12.59, 0.45,17.52	$\Omega6 > \Omega2 > \Omega4$	[6]	0.03
Molybdenum borosilicate	0.98, 0.23, 0.69	$\Omega2 > \Omega4 > \Omega6$	[33]	
Silicate	8.32, 2.14, 2.75	$\Omega2 > \Omega6 > \Omega4$	[34]	
Lead borosilicate	11.43, 4.38, 3.82	$\Omega2 > \Omega4 > \Omega6$	[35]	
Phosphate	8.05, 2.77, 2.31	$\Omega2 > \Omega4 > \Omega6$	[36]	
Silicate	8.06, 2.24, 2.03	$\Omega2 > \Omega4 > \Omega6$	[37]	

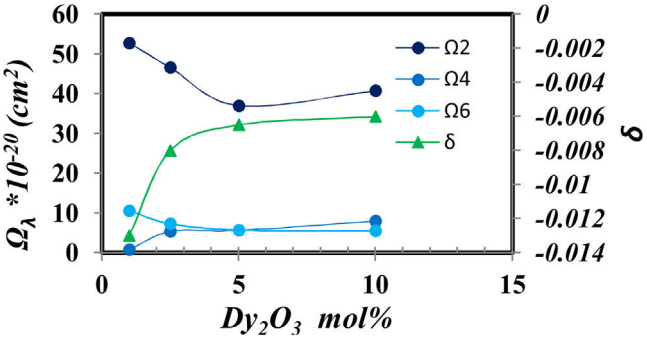

Fig. 8 – The Judd–Ofelt parameters (Ω_λ) and the bonding parameters (δ).

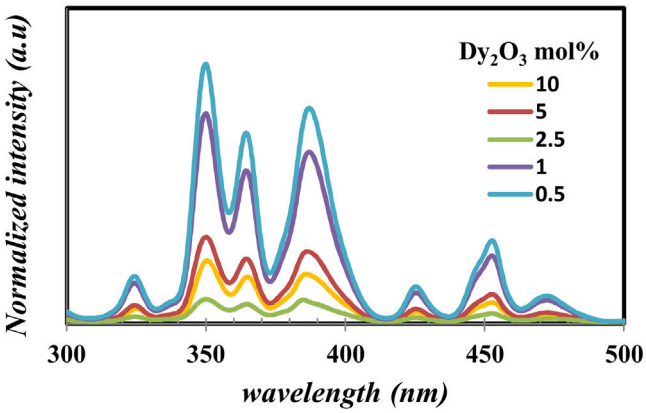

Fig. 9 – Excitation spectrum of prepared glass samples under 575 nm emission wavelength.

ters and Ω_4/Ω_6 ratio for glass samples under study compared to other glass systems as shown in Table 3.

The higher value of Ω_2 in the studied glass system indicates a moderately stronger covalence and asymmetry around the Dy^{3+} ion compared to other glass systems. A higher value of spectral quality factor $X = \Omega_4/\Omega_6$ indicates the emission of a dominant component in the gain medium. It was found that the spectral quality factor computed for the samples under study is the maximum optimal doping concentration of Dy to be 10 mol%. It is higher than the other glass systems in the literature, as shown in Table 3.

Fig. 9 displays the photoluminescence excitation of glass samples emitted under 575 nm for all prepared glass samples. For all glass samples, it observed the photoluminescence excitation bands [38] at 324, 350, 364, 386, 425, 452, and 470 nm corresponding the transition from the ground state $^6H_{15/2}$ to $^4M_{17/2} + {}^6P_{3/2}$, $^6P_{7/2}$, $^4I_{11/2} + {}^6P_{5/2}$, $^4I_{13/2} + {}^4F_{7/2}$, $^4G_{11/2}$, $^4I_{15/2}$, and $^4F_{9/2}$ excited states. It noticed the presence of nonlinearity behavior in all the exciting peaks, however, the peak position has the same energy value. The peak centered at 350, 364, and 386 nm have the highest intensity, make them appreciate for photoluminescence emission measurement.

Fig. 10 shows the emission of glass samples with different concentrations of Dy as excited with 350 nm, 370 nm, and 390 nm. The emission intensity depends mainly on the concentration of the Dy, host and the exciting energy.

Fig. 10 observed the broadness of peak and the change of intensity with any change of concentration of Dy or the change of exciting energy. The broadness of peak due to there are several Stark levels for the $^4F_{9/2}$ and ^6H_J levels [39].

With the increase of Dy concentration at excitation 370 nm, and 390 nm, it shows the splitting of peaks due to the appearance of the Stark splitting [39]. The two emission peaks assigned to 482 represented as the magnetic dipole transition corresponding to $^4F_{9/2} \rightarrow {}^6H_{15/2}$ (blue) and 574 nm represented to electric dipole transition corresponding to $^4F_{9/2} \rightarrow {}^6H_{15/2}$ (yellow) [13,40]. The strength of rare-earth ion transition ^4F–^4F transition relates to the strength parameters $[U^\lambda]_{i \rightarrow j'}$ and consequently the strength parameter depends on the host and RE ions. For Dy^{3+}, the $[U^2]$ value of the $^4F_{9/2} \rightarrow {}^6H_{13/2}$ transition about (0.049) larger than the value transition $^4F_{9/2} \rightarrow {}^6H_{13/2}$ about (0), make the emission intensity of the $^4F_{9/2} \rightarrow {}^6H_{13/2}$ transition appreciably depends on the chemical surroundings of the luminescent center [13,41]. The convergence of values between $^6H_{13/2}$ and $^6H_{15/2}$ transition shows the lower asymmetric for glasses [29]. Fig. 10 shows the increase in intensity with the increase of Dy concentration up to 1 mol% and then decrease. The decrease is a result of luminescence quenching. The luminescence quenching is explained by two mechanisms the first is the increase of the Dy–Dy distance and leads to

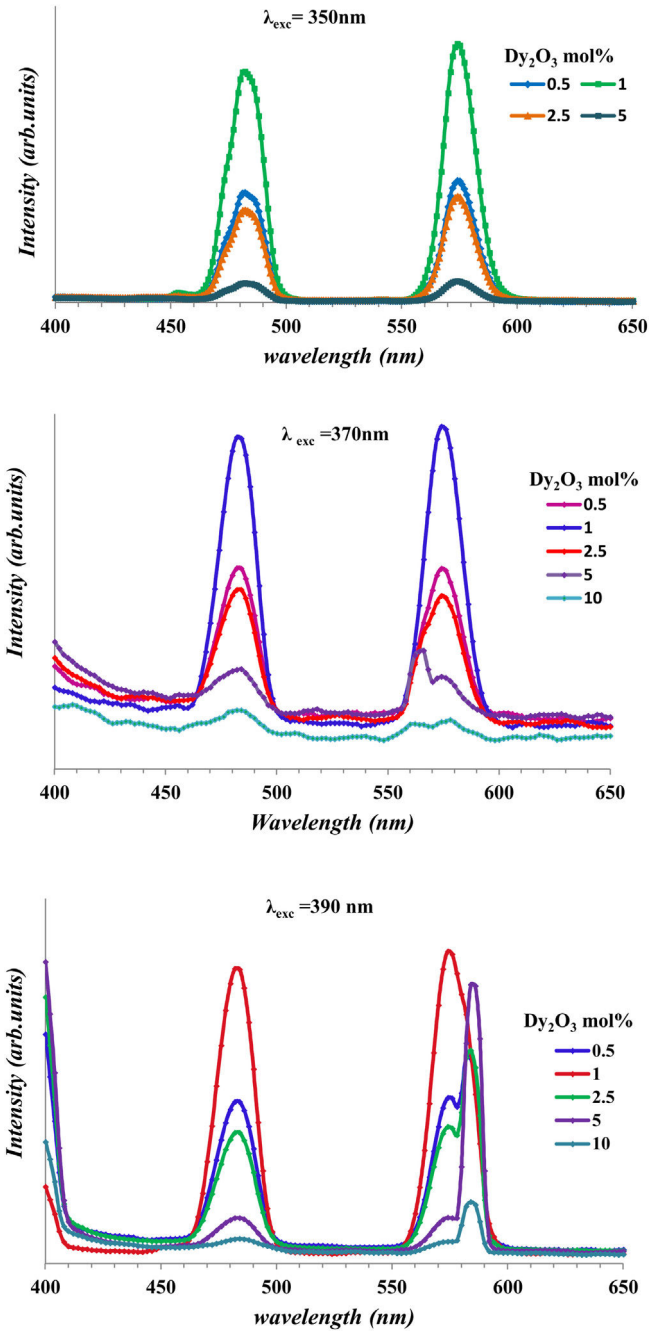

Fig. 10 – The emission of glass samples doped with different Dy^{3+} concentrations at λ_{exc} = 350 nm, 370 nm, and 390 nm.

Table 4 – The Dy ions concentration per unit volume and Dy—Dy separation.

Dy_2O_3mol%	$N \times 10^{22}$(ion/cm^3)	$R \times 10^{-8}$(cm)
0.5	1.75031	3.85149
1	0.912293	4.78581
2.5	0.389663	6.35482
5	0.209835	7.81101
10	0.116765	9.49647

the increase of nonradiative energy. The second due to the cross-relaxation mechanism [13,40,42].

The Dy—Dy separation calculated according to the relation:

$$R = \left(\frac{1}{N}\right)^{1/3} \tag{8}$$

where N is the concentration of Dy per unit volume in glass samples and determined using

$$N = \rho * Na/100W \tag{9}$$

where ρ is sample density, Na is Avogadro's number and W is the atomic weight of Dy.

R and N are tabulated in Table 4. From it observed the Dy—Dy separation increases and the N decreases as the Dy content increases which cause the luminescence quenching.

The type of quenching could be determined according to Dexter's theory. If the concentration of rare earth is large enough, draw the relation between log I/x and log x according to the relation

$$K\left[1+\beta\left(x^{\theta/3}\right)\right]^{-1} \text{ or } \log\left(\frac{I}{x}\right) = c - \left(\frac{\theta}{3}\right)\log(x) \tag{10}$$

where, K, β, and c are constant. θ = 6, 8, and 10 are corresponding to electric dipole–dipole (d–d), electric dipole–quadrupole (d–q), and electric quadrupole–quadrupole (q–q) interactions, respectively.

Fig. 11 shows the log (I/x)–log(x) plot for the $^4F_{9/2} \rightarrow {}^6H_{15/2}$ transitions of Dy^{3+} ions excited at 350 nm, 370 nm, and 390 nm. In the region of high concentrations using linear fitting the experimental data, the slope parameter equals 1.7738 and the calculated value of θ = 5.3214 near the value of 6 in two excitations 370 nm and 390 nm for glass samples. It indicates the electric dipole–dipole interaction mechanism, which different for glass samples excited at 350 nm that have θ = 7.5, near the 8 value represented as electric dipole–quadrupole (d–q) mechanism is dominant for the energy transfer among Dy^{3+} ions in glass samples, it agrees with the other studies [39,41,43].

Table 5 – Color coordinates (X, Y), CCT ratio, and Y/B ratio for glass compositions excited at 350, 370, and 390 nm.

Dy_2O_3	Y/B at (nm)			(x,y)chromaticity			CCT at (nm)		
	350	370	390	350	370	390	350	370	390
0.5	1.1	0.99	1.07	(0.34, 0.36)	(0.32, 0.33)	(0.34, 0.35)	5095	6046	5141
1	1.11	1.01	1.06	(0.36, 0.37)	(0.32, 0.34)	(0.34,0.37)	4488	5733	5147
2.5	1.13	0.95	0.99	(0.34,0.36)	(0.31, 0.32)	(0.34, 0.35)	4946	6474	4824
5	1.1	1.01	0.98	(0.35,0.31)	(0.31, 0.31)	(0.39, 0.36)	4215	6621	3497
10	–	0.73	0.79	–	(0.31, 0.30)	(0.32, 0.31)	–	6867	5942

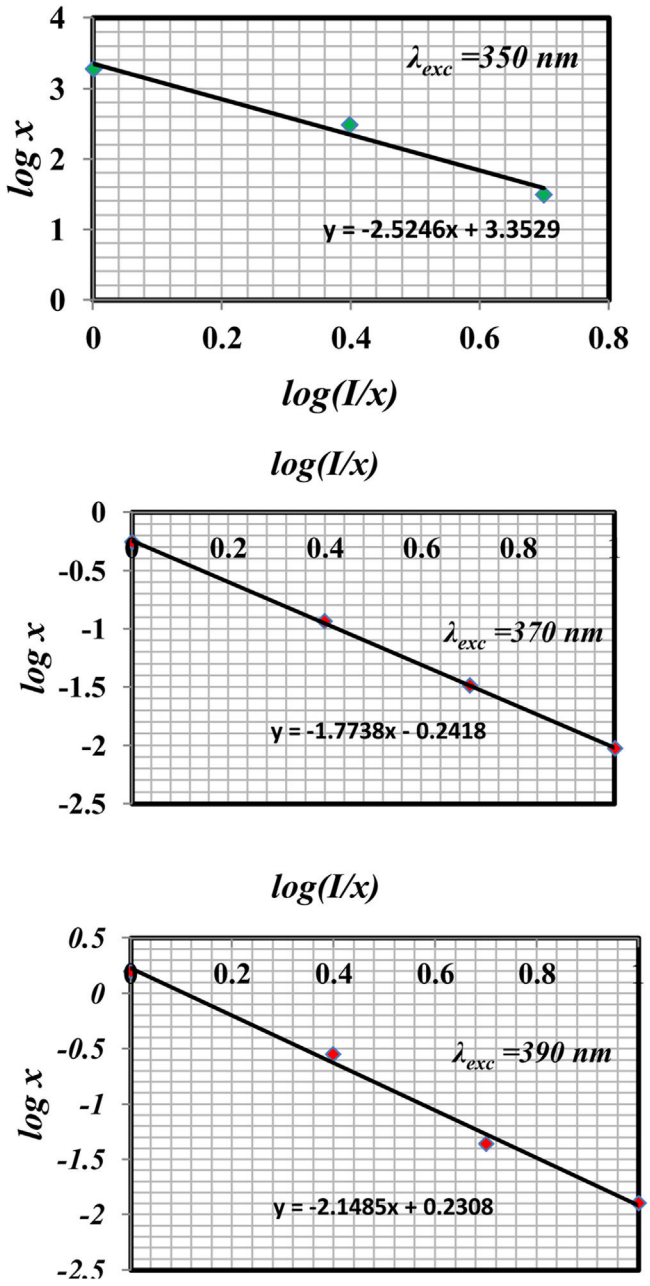

Fig. 11 – The curve of log (*I*/*x*) vs. log(*x*) of glass samples (λ_{ex} = 350, 370, and 390 nm).

The Y/B ratio clarifies the local symmetry in the lattice and the degree of iconicity or covalency between the Dy^{3+}–O^{2-} atoms.

Therefore, the alteration of Dy^{3+} concentration tunes the Y/B ratio, which aligns the chromaticity coordinates within the white light region [38].

Y/B collected in Table 5. From Table 5, the Y/B ratio of glass samples containing Dy up to 10 mol% close to unity makes it suitable for a white generation [13].

The emission spectra are used in calculating the color mapping of each sample through the chromaticity diagram.

Fig. 12 shows the CIE diagram of glass samples with different concentrations of Dy excited at 350 nm, 370nmand 390 nm.

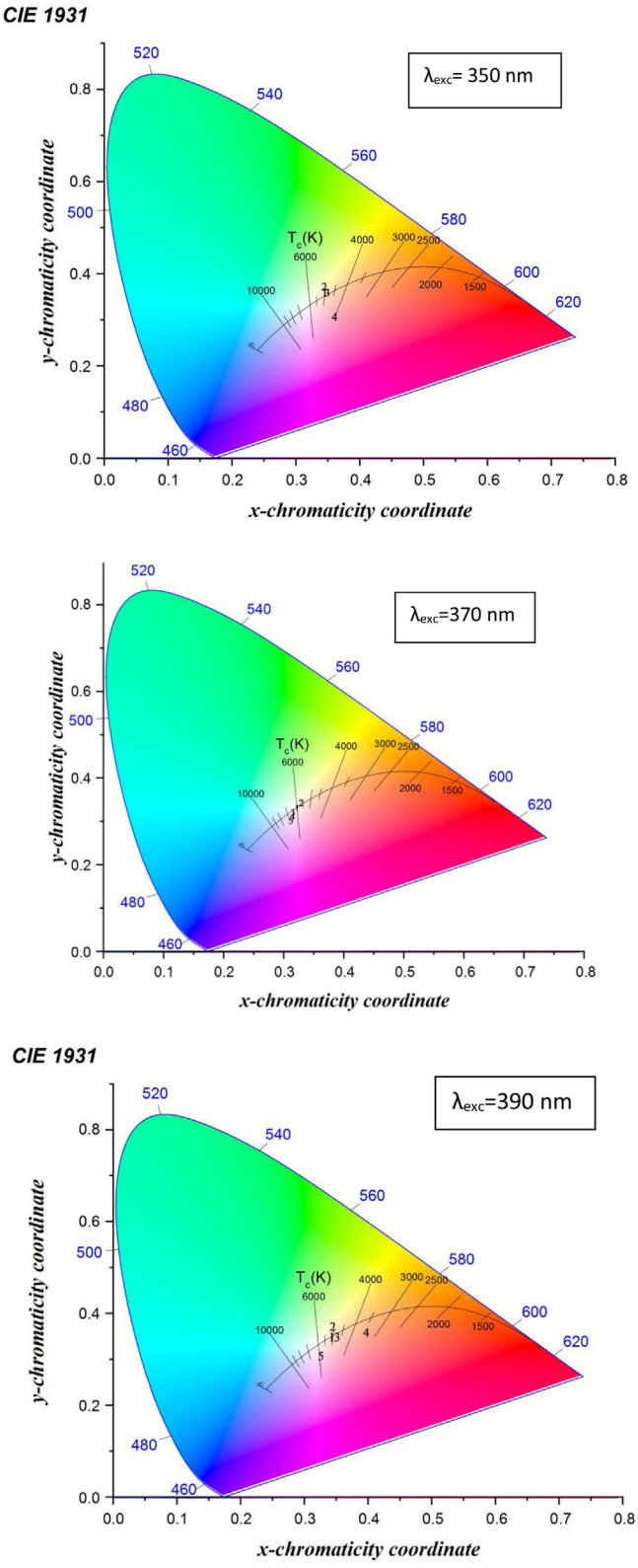

Fig. 12 – The CIE color coordinates of glass samples.

The calculated chromaticity coordinated of glass samples tabulated in Table 5. It found from the values the dependence relation between Y/B ratio and the (x, y) chromaticity [19] as when the Y/B ratio close to unity, the chromaticity values reach be ideal white illumination (0.33,0.33) [39] at the sample excited at 370 nm, the sample excited at 350 nm and 390 nm have values far enough from the white region. Further specification of white light appears in the determination of the correlated color temperature CCT. The CCT importance [13] summarized in determining the type of white color as a cold light used in official places or warm light used in a warm and relaxed places. The CCT calculated according to the relation [40,44].

$$CCT = -449n^3 + 352n^2 - 6823n + 5520.33 \quad (11)$$

where $n = (x - xe)/(y - ye)$ is the inverse slope line and ($xe = 0.332$, $ye = 0.186$) is the epicenter.

The CCT temperature calculation guides the glass sample in the application, divided according to the temperature as a warm light is around 2700 K, moving to neutral white at around 4000 K, and to cool white, at 5000 K or more. The required range of white color temperatures is from about 3000 to 9300 K, for the most typical applications, the white point is targeted to be near 6500 K (called D65) to 10,000 K [45].

Table 5 indicates the different characterization range of temperature in glass samples excited with 350 nm, 370 nm, and 390 nm. The samples with the little concentration of Dy exited with different energy behavior as the cool white, the samples at the composition 2.5 mol% Dy up to 10 mol% Dy excited at 370 nm have the D65 application, the sample at 5 mol% Dy excited at 390 nm could be explained as the natural or warm light and the sample 5 mol% Dy excited at 350 nm could be used as natural light.

Conclusion

Glasses with composition $30Li_2O–30Si_2O–(40 - x)\ B_2O_3–x$ mol% of Dy_2O_3 (where x = 0, 1, 2.5, 5 and 10 mol%) synthesized by melt quenching method. Examination of samples using X-ray diffraction confirmed the amorphous nature of the prepared glass samples.

The presence of different structural units such as BO_3, BO_4, and SiO_4 was identified by infrared spectroscopy. The J–O parameter of the prepared glass samples containing 10 mol% Dy_2O_3 content has the trend $\Omega_2 > \Omega_4 > \Omega_6$. The other samples have the trend $\Omega_2 > \Omega_6 > \Omega_4$. Higher values of Ω_2 indicate low symmetry and ionicity around the Dy^{3+} ionic site. This indicates the high quality of glass hosts for use in optoelectronic applications.

The quenching behavior was observed in glass samples containing a Dy^{3+} ion concentration above 1.0 mol%.

Through Dexter's theory, it is found that the energy transfer between Dy^{3+} ions in glass samples is due to the nature of the dipole-dipole and dipole-quadrupole interaction.

CIE coordinates were calculated for the glass samples under study.

Its values are falling in the white light region. The CCT values of the samples under study indicate the possibility of generating cold light from the prepared glass under the specified excitation. Hence some glass samples under the current study can be suitable ambitious for the development of laser as well as cool white light with excitation and adapt to the appropriate Y/B ratio.

REFERENCES

[1] T.A. Lodi, M. Sandrini, A.N. Medina, M.J. Barboza, F. Pedrochi, A. Steimacher, Dy:Eu doped CaBAl glasses for white light applications, Opt. Mater. (Amst.) 76 (2018) 231–236, http://dx.doi.org/10.1016/j.optmat.2017.12.043.

[2] S. Zulfiqar, A. Ahamed, C.M. Reddy, B.D. Prasad, Structural, thermal and optical investigations of Dy^{3+} ions doped lead containing lithium fluoroborate glasses for simulation of white light, Opt. Mater. (Amst) 35 (7) (2013) 1385–1394, http://dx.doi.org/10.1016/j.optmat.2013.02.006.

[3] O. Kıbrıslı, A.E. Ersundu, M.Ç. Ersundu, Dy^{3+} doped tellurite glasses for solid-state lighting: an investigation through physical, thermal, structural and optical spectroscopy studies, J. Non-Cryst. Solids 513 (2019) 125–136.

[4] P.P. Pawar, S.R. Munishwar, S. Gautam, R.S. Gedam, Physical, thermal, structural and optical properties of Dy^{3+} doped lithium alumino-borate glasses for bright W-LED, J. Lumin. 183 (2017) 79–88, http://dx.doi.org/10.1016/j.jlumin.2016.11.027.

[5] P. Suthanthirakumar, K. Marimuthu, Investigations on spectroscopic properties of Dy^{3+} doped zinc telluro-fluoroborate glasses for laser and white LED applications, J. Mol. Struct. 1125 (2016) 443–452, http://dx.doi.org/10.1016/j.molstruc.2016.06.080.

[6] M. Monisha, N. Mazumder, G. Lakshminarayana, S. Mandal, S.D. Kamath, Energy transfer and luminescence study of Dy^{3+} doped zinc-aluminoborosilicate glasses for white light emission, Ceram. Int. (June) (2020) 1–13, http://dx.doi.org/10.1016/j.ceramint.2020.08.167.

[7] D.D. Ramteke, R.S. Gedam, H.C. Swart, Physical and optical properties of lithium borosilicate glasses doped with Dy^{3+} ions, Phys. B Condens. Matter 535 (July 2017) (2018) 194–197, http://dx.doi.org/10.1016/j.physb.2017.07.035.

[8] D.D. Ramteke, V. Kumar, H.C. Swart, Spectroscopic studies of Sm^{3+}/Dy^{3+} co-doped lithium boro-silicate glasses, J. Non-Cryst. Solids 438 (2016) 49–58, http://dx.doi.org/10.1016/j.jnoncrysol.2016.02.010.

[9] Y.B. Saddeek, K.H.S. Shaaban, R. Elsaman, A. El-Taher, T.Z. Amer, Attenuation-density anomalous relationship of lead alkali borosilicate glasses, Radiat. Phys. Chem. 150 (April) (2018) 182–188, http://dx.doi.org/10.1016/j.radphyschem.2018.04.028.

[10] Y.B. Saddeek, M.S. Gaafar, S.A. Bashier, Structural influence of PbO by means of FTIR and acoustics on calcium alumino-borosilicate glass system, J. Non-Cryst. Solids 356 (20–22) (2010) 1089–1095, http://dx.doi.org/10.1016/j.jnoncrysol.2010.01.010.

[11] C. Zhu, D. Wu, J. Liu, M. Zhang, Y. Zhang, Color-tunable luminescence in Ce-, Dy-, and Eu-doped oxyfluoride aluminoborosilicate glasses, J. Lumin. 183 (2017) 32–38, http://dx.doi.org/10.1016/j.jlumin.2016.11.004.

[12] A. Kaur, S. Khan, D. Kumar, V. Bhatia, S.M. Rao, N. Kaur, K. Singh, A. Kumar, S. Pal Singh, Effect of MnO on structural, optical and thermoluminescence properties of lithium borosilicate glasses, J. Lumin. 219 (May 2019) (2020) 116872, http://dx.doi.org/10.1016/j.jlumin.2019.116872.

[13] L. Mishra, A. Sharma, A.K. Vishwakarma, K. Jha, M. Jayasimhadri, B.V. Ratnam, K. Jang, A.S. Rao, R.K. Sinh, White light emission and color tunability of dysprosium doped

barium silicate glasses, J. Lumin. 169 (2016) 121–127, http://dx.doi.org/10.1016/j.jlumin.2015.08.063.
[14] L.H.C. Andrade, S.M. Lima, M.L. Baesso, A. Novatski, J.H. Rohling, Y. Guyot, G. Boulon, Tunable light emission and similarities with garnet structure of Ce-doped LSCAS glass for white-light devices, J. Alloys Compd. 510 (2012) 54–59, http://dx.doi.org/10.1016/j.jallcom.2011.08.053.
[15] M. Sundara Rao, V. Sudarsan, M.G. Brik, K. Bhargavi, Ch. SrinivasRao, Y. Gandhi, N. Veeraiah, The de-clustering influence of aluminum ions on the emission features of Nd^{3+} ions in $PbO–SiO_2$ glasses, Opt. Commun. 298–299 (2013) 135–140, http://dx.doi.org/10.1016/j.optcom.2013.02.011.
[16] K.S. Shaaban, A.A. El-Maaref, M. Abdelawwad, Y.B. Saddeek, H. Wilke, H. Hillmer, Spectroscopic properties and Judd–Ofelt analysis of Dy^{3+} ions in molybdenum borosilicate glasses, J. Lumin. 196 (May 2017) (2018) 477–484, http://dx.doi.org/10.1016/j.jlumin.2017.12.041.
[17] A.A. El-Maaref, K.S. Shaaban, M. Abdelawwad, Y.B. Saddeek, Optical characterizations and Judd–Ofelt analysis of Dy^{3+} doped borosilicate glasses, Opt. Mater. (Amst) 72 (May 2018) (2017) 169–176, http://dx.doi.org/10.1016/j.optmat.2017.05.062.
[18] I. Kashif, A. Ratep, S.K. El-Mahy, Structural and optical properties of lithium tetraborate glasses containing chromium and neodymium oxide, Mater. Res. Bull. 89 (2017) 273–279, http://dx.doi.org/10.1016/j.materresbull.2017.02.006.
[19] V.P. Tuyen, V.X. Quang, P.V. Do, L.D. Thanh, N.X. Ca, V.X. Hoa, L. van Tuat, L.A. Thi, M. Nogami, An in-depth study of the Judd–Ofelt analysis, spectroscopic properties and energy transfer of Dy^{3+} in alumino-lithium-telluroborate glasses, J. Lumin. 210 (November 2018) (2019) 435–443, http://dx.doi.org/10.1016/j.jlumin.2019.03.009.
[20] I. Kashif, A. Ratep, Effect of copper addition on BO_4, H_2O groups and optical properties of lithium lead borate glass, Opt. Quant. Electron. 49 (6) (2017), http://dx.doi.org/10.1007/s11082-017-1067-7.
[21] R. Kaur, V. Bhatia, D. Kumar, S.M.D. Rao, S. Pal, Physical, structural, optical and thermoluminescence behavior of Dy_2O_3 doped sodium magnesium borosilicate glasses, Results Phys. 12 (November 2018) (2019) 827–839.
[22] M.G. Moustafa, M.Y. Hassaan, Optical and dielectric properties of transparent $ZrO_2–TiO_2–Li_2B_4O_7$ glass system, J. Alloys Compd. 710 (2017) 312–322, http://dx.doi.org/10.1016/j.jallcom.2017.03.192.
[23] E.A. Mohamed, A. Ratep, E.K. Abdel-Khalek, I. Kashif, Crystallization kinetics and optical properties of titanium–lithium tetraborate glass containing europium oxide, Appl. Phys. A Mater. Sci. Process. 123 (7) (2017), http://dx.doi.org/10.1007/s00339-017-1090-3.
[24] S. Ruengsri, J. Kaewkhao, P. Limsuwan, Optical characterization of soda lime borosilicate glass doped with TiO_2, Proc. Eng. 32 (2012) 772–779, http://dx.doi.org/10.1016/j.proeng.2012.02.011.
[25] V. Uma, K. Maheshvaran, K. Marimuthu, G. Muralidharan, Structural and optical investigations on Dy^{3+}doped lithium tellurofluoroborate glasses for white light applications, J. Lumin. 176 (2016) 15–24, http://dx.doi.org/10.1016/j.jlumin.2016.03.016.
[26] A. Balakrishna, D. Rajesh, Y.C. Ratnakaram, Structural and photoluminescence properties of Dy3 doped different modifier oxide-based lithium borate glasses, J. Lumin. 132 (11) (2012) 2984–2991, http://dx.doi.org/10.1016/j.jlumin.2012.06.014.
[27] K.V. Rao, S. Babu, G. Venkataiah, Y.C. Ratnakaram, Optical spectroscopy of Dy^{3+} doped borate glasses for luminescence applications, J. Mol. Struct. 1094 (April) (2015) 274–280, http://dx.doi.org/10.1016/j.molstruc.2015.04.015.
[28] Q. Chen, M. Zhang, Q. Ma, Q. Wang, The structure, spectra and properties of Dy_2O_3 modified diamagentic lead-bismuth-germanium glasses, J Non-Cryst. Solids 507 (September 2018) (2019) 46–55, http://dx.doi.org/10.1016/j.jnoncrysol.2018.09.025.
[29] F. Ahmadi, R. Hussin, S.K. Ghoshal, Tailored optical properties of Dy^{3+} doped magnesium zinc sulfophosphate glass: function of silver nanoparticles embedment, J. Non-Cryst. Solids 499 (May) (2018) 131–141, http://dx.doi.org/10.1016/j.jnoncrysol.2018.07.011.
[30] M. Gökçe, D. Koçyiğit, Spectroscopic investigations of Dy^{3+} doped borogermanate glasses for laser and wLED applications, Opt. Mater. (Amst.) 89 (February) (2019) 568–575, http://dx.doi.org/10.1016/j.optmat.2019.02.004.
[31] A. Kumar, D.K. Rai, S.B. Rai, Optical properties of Er^{3+} ions doped in oxyfluoroborate glass, Spectrochim. Acta – Part A Mol. Biomol. Spectrosc. 58 (14) (2002) 3067–3075, http://dx.doi.org/10.1016/S1386-1425(02)00030-6.
[32] A. Ichoja, S. Hashim, S.K. Ghoshal, I.H. Hashim, R.S. Omar, Physical, structural and optical studies on magnesium borate glasses doped with dysprosium ion, J. Rare Earths 36 (12) (2018) 1264–1271, http://dx.doi.org/10.1016/j.jre.2018.05.013.
[33] B. Nagaraja Naick, S. Damodaraiah, V. Reddy Prasad, R.P. Vijaya Lakshmi, Y.C. Ratnakaram, Judd–Ofelt analysis and luminescence studies on Dy^{3+}-doped different phosphate glasses for white light emitting material applications, Optik (Stuttg.) 192 (2019) 162980.
[34] N. Vijaya, K. Upendra Kumar, C.K. Jayasankar, Dy^{3+}-doped zinc fluorophosphate glasses for white luminescence applications, Spectrochim. Acta – Part A Mol. Biomol. Spectrosc. 113 (2013) 145–153, http://dx.doi.org/10.1016/j.saa.2013.04.036.
[35] M.R. Babu, N.M. Rao, A.M. Babu, N. Jaidass, C.K. Moorthy, L.R. Moorthy, Effect of Dy^{3+} ions concentration on optical properties of lead borosilicate glasses for white light emission, Optik (Stuttg.) 127 (5) (2016) 3121–3126.
[36] S.A. Jupri, S.K. Ghoshal, M.F. Omar, N.N. Yusof, Spectroscopic traits of holmium in magnesium zinc sulfophosphate glass host: Judd–Ofelt evaluation, J. Alloys Compd. 753 (2018) 446–456.
[37] B. Suresh, Y. Zhydachevskii, M.G. Brik, A. Suchocki, M.S. Reddy, N. Piasecki Michałand, Veeraiah, Amplification of green emission of Ho^{3+} ions in lead silicate glasses by sensitizing with Bi^{3+} ions, J. Alloys Compd. 683 (2016) 114–122.
[38] G. Lakshminarayana, K.R. Vighnesh, N.S. Prabhu, D. Lee, J. Yoon, T. Park, S.D. Kamath, Dy^{3+}:$B_2O_3–Al_2O_3–ZnF_2–NaF/LiF$ oxyfluoride glasses for cool white or day white light-emitting applications, Opt. Mater. (Amst.) 108 (July) (2020) 110186, http://dx.doi.org/10.1016/j.optmat.2020.110186.
[39] X. yuan Sun, S. ming Huang, X. san Gong, Q. chun Gao, Z. piao Ye, C. yan Cao, Spectroscopic properties and simulation of white-light in Dy^{3+}-doped silicate glass, J. Non-Cryst. Solids 356 (2) (2010) 98–101, http://dx.doi.org/10.1016/j.jnoncrysol.2009.10.009.
[40] F. Zaman, G. Rooh, N. Srisittipokakun, T. Ahmad, I. Khan, M. Shoaib, J. Ataullah, J. Rajagukguk, Kaewkha, Comparative investigations of gadolinium based borate glasses doped with Dy^{3+} for white light generations, Solid State Sci. 89 (December 2018) (2019) 50–56, http://dx.doi.org/10.1016/j.solidstatesciences.2018.12.020.
[41] Z. Yang, H. Dong, X. Liang, C. Hou, L. Liu, F. Lu, Preparation and fluorescence properties of color tunable phosphors $Ca_3Y_2(Si_3O_9)_2$:Dy^{3+}, Dalt. Trans. 43 (30) (2014) 11474–11477, http://dx.doi.org/10.1039/c4dt00794h.
[42] S. Kaura, D. Arora, S. Kumara, G. Singh, S. Mohan, P. Kaur, Kriti, P. Kaur, D.P. Singh, Blue-yellow emission adjustability with aluminium incorporation for cool to warm white light

generation in dysprosium doped borate glasses, J. Lumin. 202 (May) (2018) 168–175, http://dx.doi.org/10.1016/j.jlumin.2018.05.034.

[43] Q. Meng, B. Chena, W. Xu, Y. Yang, X. Zhao, W. Di, S. Lu, X. Wang, Size-dependent excitation spectra and energy transfer in Tb^{3+}-doped Y_2O_3 nanocrystalline, J. Appl. Phys. 102 (9) (2007) 1–7, http://dx.doi.org/10.1063/1.2803502.

[44] S. Kaur, O.P. Pandey, C.K. Jayasankar, N. Chopra, Spectroscopic, thermal and structural investigations of Dy^{3+} activated zinc borotellurite glasses and nano-glass-ceramics for white light generation, J. Non-Cryst. Solids 521 (February) (2019), http://dx.doi.org/10.1016/j.jnoncrysol.2019.119472.

[45] K.A. Bashar, W.L. Fong, K.A. Haider, S.O. Baki, M.H.M. Zaid, M.A. Mahdi, Optical studies on Tb^{3+}:Dy^{3+} singly and doubly doped Borosilicate glasses for white light and solid state lighting applications, J. Non-Cryst. Solids 534 (November 2019) (2020) 119943, http://dx.doi.org/10.1016/j.jnoncrysol.2020.119943.